ISSN 1330-3651 (Print), ISSN 1848-6339 (Online)
https://doi.org/10.17559/TV-20240222001343
Original scientific paper

# Energy-Efficient Driving Model for Intelligent Connected Vehicles Using Multi-Objective Optimization

Jiaonan LI, Changsong MA, Liang Hou, Yuzhong YAO*, Peichun CHEN

**Abstract:** This study endeavors to devise an energy-saving driving model for intelligent connected vehicles by amalgamating Deep Convolutional Neural Network (DCNN), refining Non-dominated Sorting Genetic Algorithm II (NSGA-II), and employing Model Predictive Control (MPC) algorithms, with the aim of bolstering driving sensitivity, the adaptability of intelligent solutions, and mitigating vehicle energy consumption. The study impetus stems from the pressing necessity to enhance vehicle energy efficiency, safety, and comfort. Methodologically, DCNN is employed to meticulously extract driving scene features, the NSGA-II algorithm, enhanced with adaptive crossover probability and elite preservation mechanism, is utilized to optimize multi-objective driving performance, while the MPC algorithm is tasked with formulating real-time control strategies. The study is centered on enhancing the NSGA-II algorithm and its application in energy-saving driving, questing for optimal solutions in multidimensional space across common driving scenarios through a multi-objective optimization framework. The findings indicate that: (1) In urban congestion environments, optimized vehicles demonstrate heightened energy efficiency. Specifically, the average vehicle speed increases by 25.42%, underscoring vehicles' enhanced navigability in congested environments; the average traction power consumption decreases by 11.37%, markedly curbing energy wastage. During high-speed cruising, both traction power and braking power are reduced, with the number of emergency braking instances dropping from 12 to 9, bolstering both safety and energy efficiency. (2) During parking and start-stop dynamic stages, model optimization leads to a reduction in idle total time from 60 minutes to 45 minutes, and idle fuel consumption rate decreases from 0.75 L/h to 0.62 L/h, augmenting both economy and environmental compliance. (3) In mountainous winding road environments, the optimized model exhibits enhanced climbing efficiency, decreased instances of emergency braking, and improved maneuverability, enabling drivers to experience safe and comfortable driving in complex terrains. From a practical perspective, this study proffers novel solutions for energy-saving driving of intelligent connected vehicles, contributing to reductions in energy consumption, emissions, and enhanced driving experiences. Theoretically, this study delves into the fusion of deep learning, optimization algorithms, and control theory in the realm of energy-saving driving, furnishing valuable insights for further research in related domains. Additionally, the entire study process also reflects a positive contribution to environmental protection, energy conservation, and intelligent travel, aligning with the contemporary imperatives of sustainable development era.

**Keywords:** DCNN; driving scenarios; global search; MPC; NSGA-II; multi-objective optimization

## 1 INTRODUCTION

In the rapidly evolving landscape of intelligent transportation systems, intelligent connected vehicles have garnered significant attention as a crucial component of the future of transportation [1, 2]. Traditional automotive driving models often focus on optimizing single performance indicators, such as improving vehicle power performance or reducing fuel consumption. However, in the era of intelligent connected vehicles, there are increasingly complex and diverse driving demands. Drivers need to consider not only the performance indicators of the vehicle but also aspects such as driving comfort, safety, and environmental friendliness. Therefore, building an energy-saving driving model that can comprehensively consider multiple performance indicators is particularly important [3].

Multi-objective optimization technology, as an effective mathematical tool, can achieve overall performance optimization while meeting multiple performance indicators [4]. In the automotive field, multi-objective optimization technology has been widely used in engine control, vehicle design, energy management, and other aspects. By reasonably setting optimization objectives and constraints, multi-objective optimization technology can reduce fuel consumption and emissions, improve driving comfort and safety while ensuring vehicle performance [5]. However, applying multi-objective optimization technology to the research of energy-saving driving models for intelligent connected vehicles still faces some challenges. Firstly, the driving environment of intelligent connected vehicles is complex and variable, requiring consideration of more diverse and complex performance indicators. Therefore, how to set optimization objectives and constraints reasonably, and how to construct effective optimization algorithms are key issues that this study needs to address. Secondly, the energy-saving driving model of intelligent connected vehicles needs to process a large amount of traffic information and vehicle status data in real-time, which poses higher requirements for the computational efficiency and real-time performance of the model.

In recent years, with the rapid development of intelligent transportation systems and electric vehicle technology, the application of multi-objective optimization methods in vehicle design, control, and energy management fields has become increasingly widespread. Fossati et al. (2021) endeavored to enhance the passive suspension system of vehicles by employing multi-objective optimization techniques. Their study yielded successful outcomes in reducing the vertical acceleration experienced by the driver's seat, thereby significantly enhancing driving comfort [6]. Turukmane et al. (2022) leveraged multispectral satellite image processing and integrated it with the Internet of Things (IoT). They developed a Deep Convolutional Neural Network (DCNN) capable of estimating landmarks within the images. This process provided highly accurate geographical information, which proved invaluable for intelligent transportation systems [7]. Yuan and Liu (2022) adopted a two-stage multi-objective decision-making framework, wherein various objectives such as minimum reactive power compensation loss, total cost, maintenance cost, and harmonic current distortion rate were considered. Employing the Non-dominated Sorting Genetic Algorithm II (NSGA-II), they identified the Pareto solution set for optimal passive filter configurations in ultra-high voltage systems. Furthermore, Criteria Importance Through Intercriteria Correlation (CRITIC) and Technique for Order of Preference by Similarity to Ideal Solution

(TOPSIS) methodologies were utilized in the second stage to ensure reliable and consistent analysis of decision-makers' globalized indicators, enabling the determination of target weights and selection of optimal solutions [8]. Silva et al. (2022) proposed an energy-efficient optimization fuzzy logic control approach tailored for modular all-wheel-drive vehicles, with a specific emphasis on power configurations suited for electric and hybrid electric vehicles [9]. Li et al. (2023) directed their attention to the design of axial flow compressors, employing the NSGA-II algorithm to refine performance based on computational fluid dynamics. They focused on optimizing the serial stator blade profile to meet requirements concerning high load and high-pressure ratios. This study offers valuable upgrade strategies aimed at enhancing axial flow compressor performance, thereby presenting viable solutions for automotive engine design [10].

Additionally, Wang et al. (2019) focused on the collaborative driving problem between connected vehicles and automated vehicles at signal-free intersections. They proposed a novel algorithm for coordinated control of Connected and Automated Vehicles (CAV) at signal-free intersections through mathematical modeling of conflict points and intersection layouts. The algorithm simplified complex coordination issues into a one-dimensional problem of searching for the optimal entry time and employed the Pontryagin minimum principle to control CAV, while considering vehicle constraints and reducing abruptness. Through simulation verification, the algorithm effectively achieved CAV coordination at different speeds, offering a new solution for safe and efficient driving at signal-free intersections [11]. Du et al. (2022) provided a comprehensive review of the multi-objective optimization of Energy Management Strategies (EMS) for hybrid electric vehicles. Given the significant impact of transient traffic information on vehicle driving conditions, they explored EMS optimization methods based on the fusion of traffic information and power management. By comparing rule-based and optimization-based EMS with intelligent algorithms, they analyzed the impact mechanism of traffic information on EMS and anticipated the development direction of integrating EMS with traffic information. This study provided theoretical support and practical guidance for reducing energy consumption and improving driving performance in hybrid electric vehicles [12]. Fernández-Rodríguez et al. (2021) addressed the practical situation of complex railway lines by proposing a novel search algorithm to obtain the optimal speed profile of trains under different arrival and intermediate time combinations. By utilizing the principles of particle swarm optimization and combining them with minimum energy consumption standards, the algorithm effectively avoided gaps in the Pareto front and provided decision support for railway operators in designing timetables. Simulation results demonstrated that optimizing the speed profile significantly reduced train energy consumption, showcasing the enormous potential of eco-driving in reducing railway energy consumption [13].

Existing literature research demonstrates that multi-objective optimization techniques can effectively balance multiple performance indicators, such as vehicle comfort and safety, energy efficiency, and emission reduction. This technology ensures that while optimizing for one objective, the performance of other important indicators is not compromised. Moreover, multi-objective optimization methods can flexibly address the design and control issues of complex systems. Furthermore, multi-objective optimization techniques can effectively integrate real-time data such as traffic information and vehicle status to provide decision support for vehicle control and energy management. Despite the significant achievements of multi-objective optimization technology in the automotive field, there are still some challenges. Firstly, as the complexity of vehicle systems increases, the computational complexity of multi-objective optimization problems also increases, making it an urgent issue to improve computational efficiency. Secondly, the application of deep learning technology in vehicle navigation is still in its infancy. How to combine it with multi-objective optimization techniques to achieve more precise and intelligent navigation functionality is also one of the current research hotspots.

To address the above-mentioned challenges, this study aims to further enhance the application effectiveness of multi-objective optimization in intelligent transportation systems by improving the core NSGA-II algorithm. The specific research objectives are as follows: (1) Enhancing computational efficiency: Addressing the shortcomings of the existing NSGA-II algorithm in computational efficiency, this study explores new algorithmic improvement strategies such as introducing parallel computing, optimizing algorithm parameters, etc., to enhance the computational efficiency and solution quality of the algorithm. (2) Improving energy efficiency and comfort: by comprehensively considering multiple performance indicators such as energy efficiency and comfort, this study utilizes the improved NSGA-II algorithm to perform multi-objective optimization on vehicle systems, aiming to achieve simultaneous improvements in vehicle energy efficiency and comfort. (3) Enhancing navigation accuracy: this study delves into the application of deep learning in vehicle navigation and integrates it with multi-objective optimization techniques. Through training and optimizing deep learning models, it aims to achieve more precise and intelligent vehicle navigation functionality, thereby improving the overall performance of intelligent transportation systems. (4) Real-world application validation: This study conducts experimental verification in actual traffic scenarios to evaluate the application effectiveness of the improved NSGA-II algorithm in intelligent transportation systems. Through comparison and analysis with existing technologies, the effectiveness and practicality of this research are validated.

The aim of this study is to further explore the application of multi-objective optimization in intelligent transportation systems by improving the core NSGA-II algorithm, with a particular focus on enhancing vehicle energy efficiency, comfort, and navigation accuracy. By addressing the challenges faced by existing research, this study provides new insights and methods for the development of intelligent transportation systems.

In response to the aforementioned challenges, this study endeavors to develop an energy-saving driving model tailored for intelligent connected vehicles through

multi-objective optimization. By delving into the intricacies of multi-objective optimization theory and methods and integrating them with the driving environment and attributes of intelligent connected vehicles, a pertinent energy-saving driving model is proposed. The study further investigates the model's application effects on enhancing energy efficiency, comfort, and safety. Through this study endeavor, novel insights and methodologies are presented for the advancement of energy-saving driving in intelligent connected vehicles, thereby contributing to the sustainable evolution of future transportation systems.

## 2 RESEARCH METHOD

### 2.1 NSGA-II Algorithm

In response to the aforementioned challenges, this study endeavors to develop an energy-saving driving model tailored for intelligent connected vehicles through multi-objective optimization. By delving into the intricacies of multi-objective optimization theory and methods and integrating them with the driving environment and attributes of intelligent connected vehicles, a pertinent energy-saving driving model is proposed. The study further investigates the model's application effects on enhancing energy efficiency, comfort, and safety. Through this study endeavor, novel insights and methodologies are presented for the advancement of energy-saving driving in intelligent connected vehicles, thereby contributing to the sustainable evolution of future transportation systems.

The NSGA-II algorithm has been extensively applied in multi-objective optimization problems. It classifies individuals into various layers using non-dominated sorting and utilizes a crowding distance operator to ensure diversity within each layer, ultimately identifying a well-balanced set of solutions in the Pareto optimal solution set [14-16].

NSGA-II considers multiple driving objectives in energy-efficient driving modes, such as energy efficiency and safety. Each objective is treated as an optimized dimension [17, 18]. NSGA-II employs evolutionary algorithm operations such as crossover and mutation to explore optimal solutions in a multi-dimensional space [19]. Its essence lies in gradually constructing the Pareto optimal frontier while preserving individual diversity [20]. The flow chart of the NSGA-II algorithm is depicted in Fig. 1.

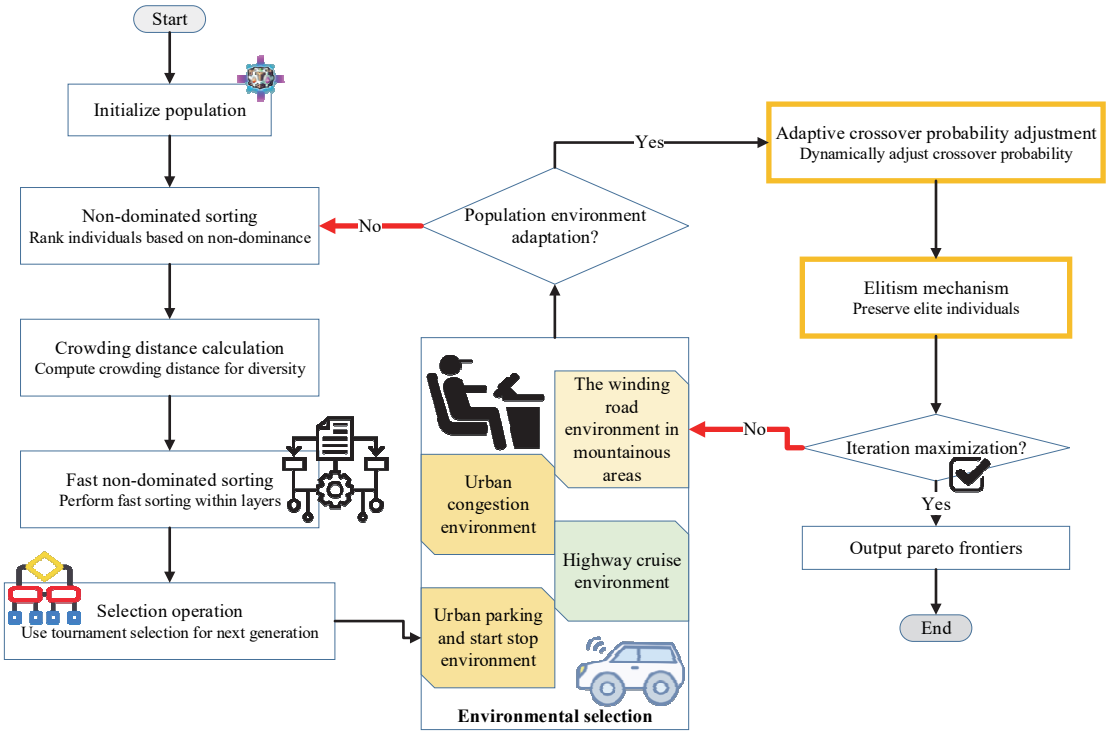


**Figure 1** Flowchart of the NSGA-II algorithm

The NSGA-II algorithm, serving as the optimization core of the energy-efficient driving model for intelligent connected vehicles, achieves multi-objective optimization based on non-dominated sorting and crowding distance calculation [21].

(1) The calculation of individual dominance relationships is shown in Eq. (1):

$$i < j \Leftrightarrow \forall k \in \{1,...,M\} : f_k(i) \le f_k(j) \wedge \exists k \in \{1,...,M\} : f_k(i) < f_k(j) \quad (1)$$

In Eq. (1), $i$ and $j$ represent individual indices. $k$ represents the index of the objective function. $M$ denotes the number of objective functions. $f_k(i)$ represents the value of individual $i$ on objective function $k$.

(2) The non-dominated sorting calculation is shown in Eq. (2):

$$Rank_i = 1 + \sum_{j=1}^{N} I_{i<j} \quad (2)$$

In Eq. (2), $N$ represents the population size. $Rank_i$ signifies the non-dominated sorting rank of individual $i$. $I_{i<j}$

is an indicator function that represents whether individual *i* dominates individual *j*.

(3) The crowding distance calculation is shown in Eq. (3):

$$Crowd_i = \sum_{j=1}^{M} \frac{f_k(P_{sorted,i+1}) - f_k(P_{sorted,i-1})}{f_k(\max) - f_k(\min)} \tag{3}$$

In Eq. (3), $P_{sorted}$ represents the set of individuals sorted according to non-dominated sorting and crowding distance. $Crowd_i$ signifies the crowding distance of individual *i*.

(4) The selection operation calculation is shown in Eq. (4):

$$Select_{Prob}(i) = \frac{Rank_i^{-1}}{\sum_{j=1}^{N} Rank_j^{-1}} \tag{4}$$

In Eq. (4), $Select_{Prob}(i)$ represents the probability of individual *i* being selected.

(5) The crossover operation calculation is shown in Eq. (5) and Eq. (6):

$$Crossover_{Prob}(i.j) = 0.5 * \left(1 + \frac{g_i - g_j}{2}\right), g_i \le 0.5 \tag{5}$$

$$Crossover_{Prob}(i.j) = 0.5 * \left(1 + \frac{2g_i}{1 + g_i - g_j}\right), g_i > 0.5 \tag{6}$$

In Eq. (5) and Eq. (6), $g_i$ represents a parameter in the crossover operation. $Crossover_{Prob}(i, j)$ indicates the probability of individuals *i* and *j* undergoing crossover.

In order to address challenges related to convergence speed and global search, the study introduces adaptive crossover probability and an elite retention mechanism, dynamically adjusting the crossover probability and maintaining elite diversity.

(6) The calculation of adaptive crossover probability is shown in Eq. (7):

$$Crossover_{Prob}(t+1) = \frac{Crossover_{Prob}(t)}{1 + \exp(\frac{F_{Obj}(t) - F_{Obj}(t-1)}{\alpha})} \tag{7}$$

In Eq. (7), $Crossover_{Prob}(t + 1)$ represents the crossover probability for the next generation. $F_{Obj}^{(t)}$ denotes the average fitness value of the population in generation *t*. $\alpha$ is a parameter for adjusting adaptability.

(7) The calculation of the elite retention mechanism is shown in Eq. (8):

$$Elitism_{Prob}(t+1) = \frac{Elitism_{Prob}(t)}{1 + \exp\left(\frac{Crowd_{Avg}^{(t)} - Crowd_{Avg}^{(t-1)}}{\beta}\right)} \tag{8}$$

In Eq. (8), $Elitism_{Prob}(t + 1)$ represents the elite retention probability for the next generatio. $Crowd_{Avg}^{(t)}$ denotes the average crowding distance of the population in generation *t*. $\beta$ is a parameter related to elitism.

## 2.2 DCNN

Mainly based on Convolutional Neural Networks (CNN), the input data is processed layer by layer through components such as convolutional layers, pooling layers, and fully connected layers to extract features [22]. DCNN estimates image landmarks within IoT integration, enabling high-precision geographical information extraction and more accurate identification of specific location resources [25].

(1) The calculation of input layer is shown in Eq. (9):

$$X^{(0)} = [x_1^{(0)}, x_2^{(0)}, ..., x_n^{(0)}] \tag{9}$$

In Eq. (9), $X^{(0)}$ represents the input to the input layer.

(2) The calculation of convolutional layer is shown in Eq. (10):

$$Z_i^{(l)} = \sum_{b=1}^{m} \sum_{k=1}^{m} (W_{ijk}^{(l)} * X_{jk}^{(l-1)}) + b_i^{(l)} \tag{10}$$

In Eq. (10), $Z_i^{(l)}$ represents the weighted input of the *i*-th neuron in layer *l*. $W_{ijk}^{(l)}$ denotes the convolutional kernel weight. $b_i^{(l)}$ represents the bias term.

(3) The calculation of nonlinear activation function is shown in Eq. (11) and Eq. (12):

$$A_i^{(l)} = Z_i^{(l)}, Z_i^{(l)} > 0 \tag{11}$$

$$A_i^{(l)} = \partial * Z_i^{(l)}, Z_i^{(l)} \le 0 \tag{12}$$

In Eq. (11) and Eq. (12), $A_i^{(l)}$ represents the activation value of the *I* th neuron in layer *l*. $\partial$ denotes the slope parameter in the nonlinear activation function [26].

(4) The calculation of batch normalization is shown in Eq. (13):

$$\widehat{A}_i^{(l)} = \frac{A_i^{(l)} - \mu_i^{(l)}}{\sigma_i^{(l)^2} + \rho} \tag{13}$$

In Eq. (13), $\widehat{A}_i^{(l)}$ represents the normalized activation value after batch normalization. $\mu_i^{(l)}$ and $\sigma_i^{(l)^2}$ respectively denote the mean and variance in batch normalization. $\rho$ represents a small constant in batch normalization to prevent division by zero [27].

(5) The calculation of spatial dropout is shown in Eq. (14):

$$\widetilde{A}_i^{(l)} = \widehat{A}_i^{(l)} \odot D_i^{(l)} \tag{14}$$

In Eq. (14), $\widetilde{A}_i^{(l)}$ represents the activation value after spatial dropout. $\odot$ denotes element-wise multiplication. $D_i^{(l)}$

represents the binary mask for spatial dropout.

(6) The calculation of two-dimensional max pooling is shown in Eq. (15):

$$P_{ij}^{(l)} = \max(\tilde{A}_{(2i-1)(2j-1)}^{(l)}, \tilde{A}_{(2i-1)(2j)}^{(l)}, \tilde{A}_{2i(2j-1)}^{(l)}, \tilde{A}_{(2i)(2j)}^{(l)}) \quad (15)$$

In Eq. (15), $P_{ij}^{(l)}$ represents the output after two-dimensional max pooling.

(7) The calculation of multi-channel convolutional layer is shown in Eq. (16):

$$Z_i^{(l+1)} = \sum_{c=1}^{C}\sum_{j=1}^{m}\sum_{k=1}^{m}(W_{ijkc}^{(l)} * P_{jk}^{(l)}) + b_i^{(l+1)} \quad (16)$$

In Eq. (16), $C$ represents the number of input channels. $Z_i^{(l+1)}$ represents the output of the multi-channel convolutional layer.

(8) The calculation of fully connected layer is shown in Eq. (17):

$$O_k^{(L)} = \delta\left(\sum_{i=1}^{n} W_{ki}^{(L)} * P_i^{(l-1)} + b_k^{(L)}\right) \quad (17)$$

In Eq. (17), $\delta$ represents the activation function in the fully connected layer. $L$ denotes the total number of layers in the network. $O_k^{(L)}$ represents the output of the k-th neuron in the output layer. $W_{ki}^{(L)}$ denotes the weight of the fully connected layer.

### 2.3 MPC Control Algorithm

The fundamental concept underlying Model Predictive Control (MPC) revolves around the optimization of a series of forthcoming control inputs at each control instance to minimize an objective function, thereby facilitating proficient control over the system [29]. Within the context of this investigation, MPC is employed for the prediction and adaptation of control inputs within dynamic environments, thereby offering enhanced efficiency, safety, and energy conservation in control strategies across varied driving scenarios.

(1) The calculation of the objective function is shown in Eq. (18):

$$J[U] = \sum_{t=0}^{N-1}\left[\left\|e_t\right\|_Q^2 + \left\|u_t\right\|_R^2\right] + \left\|e_N\right\|_{Q_N}^2 \quad (18)$$

In Eq. (18), $J[U]$ represents the objective function, representing the cost function to be minimized in the MPC optimization problem. $U$ is the control input sequence. $e_t$ represents the control error, indicating the current state deviation. $Q$, $R$ and $Q_N$ are weight matrices used to penalize the state and control input in the objective function. $N$ represents the number of optimization time steps.

(2) The calculation of discrete-time linear process is shown in Eq. (19):

$$x_{t+1} = Ax_t + Bu_t \quad (19)$$

In Eq. (19), $x_t$ represents the current state at time $t$. $A$, $B$ represent the state transition matrices in the discrete-time linear process. $u_t$ represents the current control input.

(3) The constraint conditions are shown in Eq. (20):

$$x_t \in S, u_t \in D, Fx_t + Gu_t \le h \quad (20)$$

In Eq. (20) $S$ and $D$ represent the constraint sets for state and input, respectively. $Fx_t + Gu_t$ represents the linear inequality in the constraint conditions. $h$ represents the upper limit of the constraint conditions.

### 2.4 Experimental Design

This study integrates DCNN, an enhanced NSGA-II, and MPC algorithm to formulate an intelligent connected vehicle energy-efficient driving model aimed at optimizing energy-efficient driving performance in intelligent connected vehicles through multi-objective optimization. Primarily, DCNN is employed for deep learning-based feature extraction from vehicle perceptual data, enabling precise capture of environmental information. Subsequently, to address shortcomings inherent in traditional NSGA-II, such as slow convergence and suboptimal convergence, the improved NSGA-II algorithm is introduced. This enhancement incorporates adaptive crossover probability and an elite retention mechanism, dynamically adjusting crossover probability in each generation to effectively balance global exploration and local exploitation. Moreover, the elite retention mechanism sustains population diversity, expedites convergence, enhances search efficiency, and ensures adaptability of optimal solutions across diverse scenarios [30]. In the adaptation phase, the MPC control algorithm is deployed to refine the obtained solutions, optimizing multiple objectives encompassing energy efficiency, safety, comfort, and precise parking.

The parameters of the intelligent connected sedan utilized in this investigation are detailed in Tab. 1.

**Table 1** Car parameters

| Type | Parameter name | Value |
|---|---|---|
| Kinetic parameters | vehicle quality | 1600 kg |
| | center of mass height | 0.45 m |
| | motor maximum power | 120 kW |
| | wheel radius | 0.34 m |
| | maximum braking force | 9000 N |
| | vehicle air resistance coefficient | 0.33 |
| | vehicle rolling resistance coefficient | 0.014 |
| | drive motor efficiency | 0.92 |
| | braking system efficiency | 0.85 |
| | drive motor torque characteristics | Positive linear |
| | brake system pressure | 160bar |
| Kinematic and environmental parameters | high speed and stable steering coefficient | 0.035 |
| | low-speed stable steering coefficient | 0.055 |
| | vehicle air resistance coefficient | 0.33 |
| | vehicle rolling resistance coefficient | 0.014 |
| | vehicle speed limit | 200 km/h |
| | brake sensitivity | 0.018 |

Accurate vehicle parameters contribute significantly to

enhancing model precision, ensuring that simulation outcomes closely align with real-world conditions, thereby optimizing driving strategies. For instance, improvements in transmission system efficiency can directly reduce energy consumption, while enhancements in aerodynamic design can diminish driving resistance, thereby enhancing fuel economy. Inaccurate or variable vehicle parameters, such as tire wear or engine aging, can lead to inaccuracies in optimization results. Furthermore, disparities in parameters among different vehicle models can also affect the universality of the model. In the energy-saving driving mode of intelligent connected vehicles, common scenarios are shown in Tab. 2.

Different driving scenarios impose varying demands on energy consumption and driving strategies. By conducting simulations across multiple scenarios, it becomes possible to comprehensively assess the adaptability and performance of optimization algorithms. For instance, in urban road settings, frequent stopping and starting necessitate optimization of acceleration and deceleration strategies, whereas maintaining a consistent speed is crucial for energy efficiency on highways. The complexity of real-world driving environments far surpasses the parameters set in simulations. Unforeseen circumstances, such as sudden accidents or extreme weather conditions, not accounted for in simulations, may result in optimization outcomes diverging from actual performance. The parameter ratio of the urban congestion environment is shown in Tab. 3.

**Table 2** Common driving scenarios

| Scenes | Features | Related parameters |
|---|---|---|
| Urban congestion environment | High traffic density and large speed fluctuations | Traction characteristic function, braking characteristic function, emergency braking control, start and stop frequency, step length |
| Highway cruising environment | Smooth driving at high speed | Traction characteristic function, air resistance, wind resistance characteristics, cruise speed control, power distribution |
| Urban parking and start-stop dynamic stage environment | Frequent stops and starts | Engine start and stop control, idle fuel consumption, start and stop frequency, start and stop time control. |
| Mountain winding road environment | Twist mountain road, ups and downs. | Terrain characteristics, dynamic power distribution, climbing power control, vehicle speed adjustment |

**Table 3** Urban congestion environment parameters

| Scenes | Division | Parameter | | | | |
|---|---|---|---|---|---|---|
| urban congestion environment | Period | Traction characteristic function | Braking characteristic function | Emergency braking control | Start and stop frequency | step length |
| | Morning peak | Strong - 1.2 | Weak - 0.8 | Strong - 1.5 | High - 0.8 | 0.05 second |
| | Smooth at noon | Moderate - 1.0 | Moderate - 1.0 | Moderate - 1.0 | Medium - 0.5 | 0.2 second |
| | Afternoon peak | Strong - 1.2 | Weak - 0.8 | Strong - 1.5 | High - 0.8 | 0.05 second |
| | Evening trough | Energy saving - 0.8 | Energy saving - 0.9 | Weak - 1.2 | Low - 0.2 | 0.8 second |

These parameters influence the vehicle's driving speed and frequency of acceleration and deceleration. In congested environments, optimizing driving models requires a focus on reducing idle time and frequent acceleration and deceleration to enhance fuel efficiency and reduce emissions. For example, optimizing traffic signal cycles and implementing advance deceleration strategies can reduce the number and duration of stops. The dynamic and unpredictable nature of urban congestion poses challenges for simulation models, which may not fully capture the variability of real-world conditions, resulting in diminished optimization effectiveness in practical applications. The parameter configuration of the highway cruising environment is shown in Tab. 4.

**Table 4** Highway cruising environmental parameters

| Scene | Division | Parameter | | | | |
|---|---|---|---|---|---|---|
| Highway cruising environment | State | Traction characteristic function | Aerodynamic Resistance | Wind resistance characteristics | Cruise speed control | Power distribution |
| | Smooth cruising | Moderately linear | 0.28 | Smooth | Fixed speed (100 km/h) | Equally distributed |
| | Ramp climb | Strong linearity | 0.35 | Rise | Fixed speed (80 km/h) | Dynamic Distribution (60% front wheels, 40% rear wheels) |
| | High-speed overtaking | Efficient linearity | 0.3 | High speed | Dynamic speed adjustment (120 km/h is the target speed) | Rear wheel Power enhancement (20% increase) |

On highways, vehicles typically cruise at higher speeds, with energy consumption primarily influenced by aerodynamic drag and tire rolling resistance. Optimization models need to enhance efficiency by maintaining appropriate cruising speeds and minimizing unnecessary acceleration and deceleration. For example, in windy conditions, adjusting vehicle speed to reduce aerodynamic drag can significantly lower energy consumption. Sudden events such as emergency braking and traffic accidents, as well as variations in environmental factors like wind speed and direction, may not be fully reflected in simulations on highways, impacting the practical applicability of optimization outcomes. Tab. 5 shows the parameter configuration of urban parking and start-stop dynamic phase environment.

The dynamic phases of urban parking and start-stop significantly impact a vehicle's fuel consumption. Optimization models need to reduce unnecessary idle time and start-up instances through intelligent start-stop technology and anticipatory driving strategies. For example, leveraging vehicle-to-infrastructure (V2I) technology to obtain traffic signal information in advance and optimize parking and start-up strategies can significantly enhance fuel economy. The randomness of urban traffic signals and the unpredictability of driver behavior may render the model unable to fully capture real-world conditions, affecting optimization effectiveness.

**Table 5** Environmental parameters during urban parking and start-stop dynamic phases

| Scene | Division | Parameter | | | |
|---|---|---|---|---|---|
| Urban parking and start-stop dynamic stage environment | state | Engine start/stop control | Idle Fuel Consumption | Start and stop frequency | Start and stop time control |
| | parking in heavy traffic | Intelligent control (according to traffic flow) | 0.5 L/h | High (every 2 minutes) | Dynamic adjustment (according to waiting time) |
| | parking and waiting in line | Timing control (every 5 minutes) | 0.7 L/h | Medium (every 4 minutes) | Fixed duration (3 minutes each time parking) |
| | short stops and frequent starts and stops | Active control (not less than 1min) | 0.6 L/h | Very high (every 1 minute) | Fixed duration (2 minutes each time parking) |

Tab. 6 shows the parameter ratio of winding road environment in mountainous areas:

**Table 6** Environmental parameters of winding roads in mountainous areas

| Scene | Division | Parameter | | | |
|---|---|---|---|---|---|
| Mountain winding road environment | State | terrain characteristics | Dynamic power distribution | Climb power control | Vehicle speed adjustment |
| | Smooth uphill | gentle | Rear-wheel drive first | Constant power | Dynamic Adjustment |
| | Rapid downhill | steep | Precursor first | Constant speed | Fixed speed (30km/h) |
| | curve climb | winding | All-wheel drive balanced | Adjustable power | Dynamic Adjustment |
| | Sharp turn on the mountain road | bending | Rear-wheel drive first | Adapt to slope | Dynamic adjustment (corner angle) |
| | Smooth cruising in the mountains | changeable | All-wheel drive balanced | Adaptive | Dynamic adjustment (according to traffic conditions) |

On mountainous roads, frequent turning and driving uphill and downhill pose higher demands on energy consumption and safety. Optimizing models need to control speed and acceleration reasonably while ensuring driving safety to reduce energy consumption. For instance, utilizing engine braking on downhill sections to reduce brake usage and optimizing acceleration strategies on uphill sections to enhance fuel efficiency. Mountainous road conditions are complex and variable, and simulation parameters may not fully reflect actual road conditions, especially extreme weather and sudden geological disasters. This situation may result in decreased effectiveness of optimization results in practical applications.

The selection rationale for the weight matrix in the MPC objective function mainly includes balancing energy consumption with comfort, safety considerations, and environmental factors. The weight matrix is used to balance different objectives such as energy consumption, comfort, and safety, determining reasonable weight ratios through simulation experiments and actual tests to ensure energy savings while maintaining high levels of passenger comfort and safety. Additionally, considering external environmental factors such as road conditions and traffic flow, adjusting the weights of energy saving and comfort appropriately in different environments ensures efficient vehicle operation under various conditions. For the slope parameters in the activation functions of DCNN, their selection primarily affects the stability of network training, convergence speed, and overfitting issues. Appropriate slope parameters can affect the gradient of the activation function, thereby ensuring the stability of network training and speeding up convergence. For example, the slope parameter in the ReLU activation function is typically set to 0 to ensure an output of 0 when the input is negative, reducing the likelihood of gradient vanishing. A proper slope (e.g., 0.01) in Leaky ReLU prevents neurons from completely failing during training. Choosing suitable slope parameters through methods like cross-validation can accelerate the convergence speed of the training process, reduce training time, prevent overfitting caused by excessively large slope parameters, and improve generalization ability.

NSGA-II algorithm may be less efficient in handling high-dimensional objective optimization problems, and reliance on population diversity may lead to local optimal solution problems. Assuming the objective function of the problem is differentiable and computationally inexpensive. For DCNN, a large amount of annotated data is required for training. Insufficient data may lead to decreased model performance, and the complex network structure and long training time make it prone to overfitting. DCNN assumes that input data has certain spatial structural characteristics suitable for convolution operations; otherwise, its performance may be inferior to other models. On the other hand, MPC control algorithm may have heavy computational burden in real-time applications, and real-time performance may be limited. For nonlinear and large-scale systems, MPC's computational complexity is high. It assumes the system model is accurate, and future predictions can be based on the current state and control inputs; otherwise, performance may significantly decline.

## 3 RESULTS

### 3.1 Performance Analysis in Urban Congestion Environment

"A" represents the pre-optimization phase, and "B" represents the post-optimization period. The depicted outcomes of diverse parameter indicators across various time intervals within an urban congestion setting are illustrated in Fig. 2.

In Fig. 2, the driving performance of the optimized intelligent connected vehicle demonstrates significant enhancements across various stages. Specifically, during the morning peak period, traction power consumption post-optimization registers at 9876 kJ, compared to 11345 kJ pre-optimization. Additionally, the occurrences of abrupt braking have decreased from 17 to 13, while speed has surged from 16 km/h to 22 km/h. Furthermore,

parking duration has diminished from 26 minutes to 21 minutes, alongside a reduction in idle time from 12 minutes to 6 minutes. This optimization has yielded notable improvements in energy efficiency and a marked reduction in abrupt braking incidents.

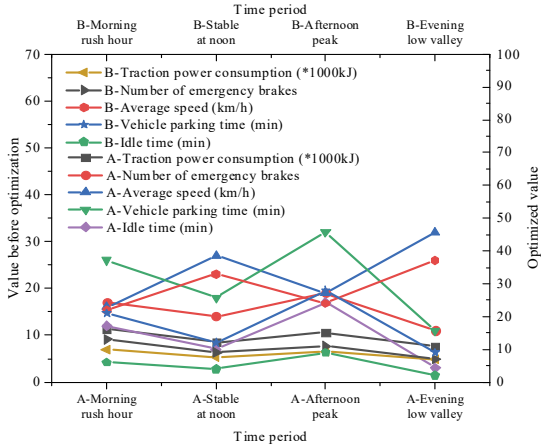


**Figure 2** Results of parameter calculations in different time periods

The performance disparities in urban congestion environments across different time segments before and after optimization are depicted in Fig. 3.

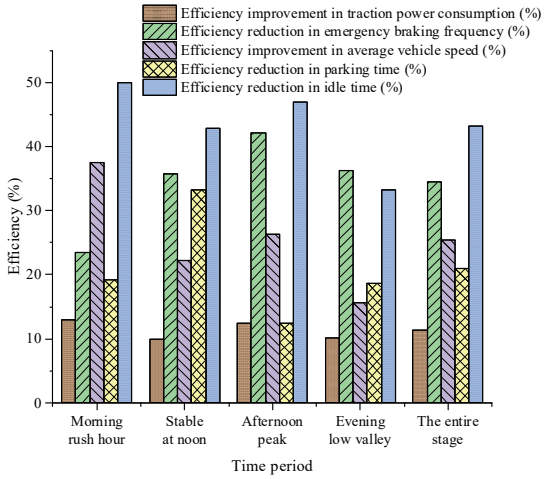


**Figure 3** Performance analysis results of various indicators in different time periods

In Fig. 3, subsequent to optimization, the average traction power consumption has exhibited an enhancement of 11.37% across the entire stage. Furthermore, the average vehicle speed has experienced a notable increase of 25.42%. Moreover, optimization efforts have yielded a remarkable reduction of 34.43% in abrupt braking incidents, alongside substantial decreases in both vehicle parking time and idle time. These enhancements underscore that, in comparison to pre-optimization conditions, the optimized intelligent connected vehicle achieves a driving state that is more efficient, safe, comfortable, and precise within urban congestion environments.

### 3.2 Performance Analysis in Highway Cruise Environment

The computed outcomes of various parameter indicators across different conditions within the highway cruise environment are delineated in Fig. 4.

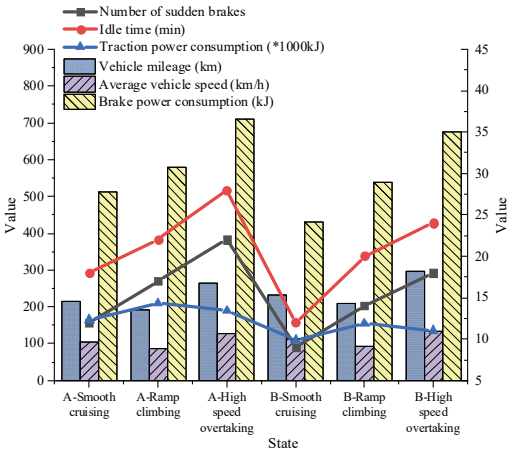


**Figure 4** Results of parameter calculations in different states

In Fig. 4, the driving performance of the optimized intelligent connected vehicle exhibits significant enhancements in smooth cruising, hill climbing, and high-speed overtaking. Prior to and subsequent to optimization in the smooth cruising state, traction power consumption has notably decreased from 12345 kJ to 9876 kJ. Concurrently, the occurrences of abrupt braking incidents have diminished from 12 to 9, while the speed has escalated to 112 km/h. Furthermore, idle time has decreased to 12 minutes, and driving distance has extended to 232 km. These optimizations have resulted in energy conservation and enhanced vehicle travel efficiency.

The performance disparities across different conditions within the highway cruise environment before and after optimization are depicted in Fig. 5.

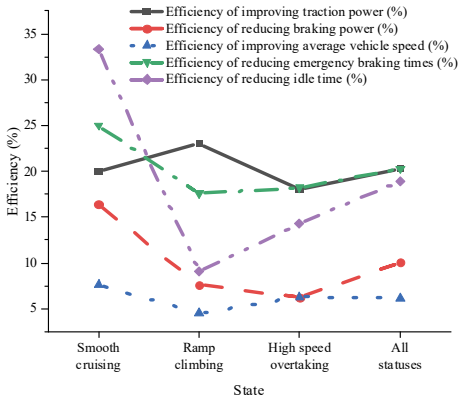


**Figure 5** Performance analysis results of various indicators in different states

In Fig. 5, within the smooth cruising state, notable reductions in traction power and braking power consumption are observed alongside an increase in speed, decrease in abrupt braking incidents, and reduction in idle time. These outcomes reflect heightened energy efficiency and comfort. In the hill climbing state, the optimized vehicle demonstrates enhanced climbing efficiency, reduced braking power, and fewer abrupt braking incidents. Furthermore, in the high-speed overtaking state, significant decreases in both traction power and braking power consumption are noted, accompanied by a substantial increase in average speed. These findings underscore the

optimized model's ability to enhance vehicle performance while ensuring efficient energy utilization, thereby highlighting its comprehensive advantages across multiple driving objectives.

### 3.3 Performance Analysis in Urban Parking and Start-Stop Dynamic Stage Environment

The performance variations across different states within the urban parking and start-stop dynamic stage environment are depicted in Fig. 6.

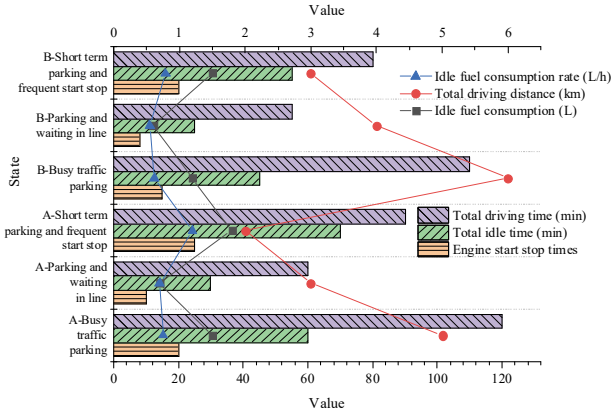


**Figure 6** Performance analysis results in urban parking and start-stop dynamic stage environment

In Fig. 6, the optimized intelligent connected vehicle exhibits noteworthy enhancements in performance amidst congested traffic scenarios, encompassing parking, queueing, and instances of frequent brief halts. There is a discernible reduction in the frequency of engine start-stop events, a concomitant decrease in total idle duration, and a pronounced diminishment in idle fuel consumption rate. Specifically, during congested traffic parking scenarios, the incidence of engine start-stop events diminishes from 20 to 15, total idle time contracts from 60 minutes to 45 minutes, idle fuel consumption diminishes from 1.5 liters to 1.2 liters, and the idle fuel consumption rate experiences a marked decline from 0.75 liters per hour to 0.62 liters per hour.

### 3.4 Performance Analysis in Mountainous Winding Road Environment

The performance disparities across various states within the mountainous winding road environment are delineated in Fig. 7.

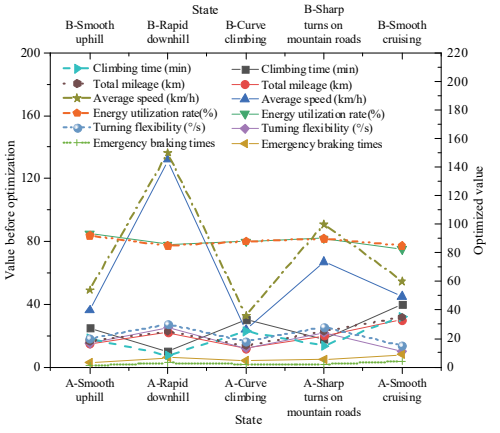


**Figure 7** Performance analysis results in mountainous winding road environment

In Fig. 7, the energy-saving driving model, subsequent to optimization, demonstrates substantial enhancements across various driving scenarios prevalent in mountainous terrain. These include stable uphill traversal, swift downhill descents, negotiating curves, navigating sharp mountainous turns, and maintaining smooth cruising. Notably, the duration required for uphill ascents diminishes, overall mileage accrues, average velocity escalates, energy utilization experiences marked amelioration, instances of sudden braking diminish, and maneuvering agility amplifies.

### 3.5 Sensitivity Analysis

In order to deepen our understanding of the robustness of the proposed model and to provide guidance for the selection of optimal parameter settings across various driving scenarios, sensitivity experiments have been undertaken. The findings of these experiments are outlined in Tab. 7.

**Table 7** Sensitivity analysis results

| Experiment No. | NSGA-II Population Size | NSGA-II Iterations | DCNN Learning Rate | DCNN Activation Function Slope | MPC Prediction Horizon | MPC Control Horizon | Total Energy Consumption / L/100 km | Average Comfort Rating (1-10) | Average Travel Time / minutes |
|---|---|---|---|---|---|---|---|---|---|
| 1 | 50 | 100 | 0.001 | 0.01 | 10 | 5 | 6.5 | 8.5 | 35 |
| 2 | 100 | 100 | 0.001 | 0.01 | 10 | 5 | 6.3 | 8.7 | 34 |
| 3 | 50 | 200 | 0.001 | 0.01 | 10 | 5 | 6.4 | 8.6 | 34.5 |
| 4 | 50 | 100 | 0.01 | 0.01 | 10 | 5 | 6.8 | 7.9 | 35.5 |
| 5 | 50 | 100 | 0.001 | 0.1 | 10 | 5 | 6.7 | 8.0 | 35.2 |
| 6 | 50 | 100 | 0.001 | 0.01 | 20 | 5 | 6.4 | 8.5 | 34.8 |
| 7 | 50 | 100 | 0.001 | 0.01 | 10 | 10 | 6.3 | 8.6 | 34.7 |
| 8 | 100 | 200 | 0.01 | 0.1 | 20 | 10 | 6.1 | 8.2 | 33 |
| 9 | 100 | 200 | 0.01 | 0.1 | 15 | 7 | 6.2 | 8.3 | 33.5 |

In Tab. 7, data from experiments 1, 2, 3, 8, and 9 are employed to assess the sensitivity of NSGA-II population size and iteration count. The analysis reveals that augmenting the population size from 50 to 100 correlates with a decrease in total energy consumption from 6.5 L/100 km to 6.3 L/100 km, an elevation in average comfort rating from 8.5 to 8.7, and a marginal decrease in average travel time. This underscores the potential of enlarging the population size to bolster optimization outcomes. However, simultaneous increments in both

population size and iteration count can engender escalated computational demands and resource utilization, necessitating a delicate equilibrium between performance enhancement and computational overhead. Data from experiments 1, 4, 5, 8, and 9 are scrutinized to explore the sensitivity of DCNN learning rate and activation function slope. The findings demonstrate that higher learning rates (e.g., 0.01 in experiment 4) correlate with heightened total energy consumption and diminished average comfort rating, suggesting that excessively elevated learning rates may precipitate instability in network training, resulting in suboptimal solutions. The activation function slope exerts a notable influence on the outcomes, with higher slopes (e.g., 0.1 in experiment 5) significantly amplifying energy consumption and reducing comfort rating. Hence, meticulous attention to the configuration of learning rate and activation function slope is imperative when selecting DCNN parameters to strike a balance between training velocity and optimization efficacy. Data from experiments 1, 6, 7, 8, and 9 are analyzed to assess the sensitivity of MPC prediction horizon and control horizon. The results indicate that expanding both prediction and control horizons (e.g., a prediction horizon of 20 and a control horizon of 10 in experiment 8) can markedly curtail total energy consumption (from 6.5 L/100 km to 6.1 L/100 km) and enhance comfort rating. This phenomenon arises from the extended prediction and control horizons enabling the model to comprehensively evaluate future states and optimize control strategies. Nonetheless, protracted horizons concomitantly escalate computational complexity and real-time requisites, necessitating a delicate balance between optimization efficacy and computational burden.

### 3.6 Performance Comparison Experiment

To investigate the advantages of the optimization algorithm proposed in this study, performance comparison experiments are conducted, juxtaposing the DRL (Deep Reinforcement Learning) and FLC (Fuzzy Logic Control) models. Evaluation metrics encompass comfort rating, safety event count, average computation time, and model stability. The experimental outcomes are delineated in Tab. 8.

**Table 8** Performance comparison results

| Metric | Proposed Optimization Model | DRL | FLC |
|---|---|---|---|
| Average Comfort Rating (1-10) | 8.7 | 8.5 | 8.0 |
| Safety Event Count / per 1000 km | 0.5 | 1.0 | 1.5 |
| Average Computation Time / milliseconds | 45 | 120 | 35 |
| Model Stability Rating (1-10) | 9.0 | 7.5 | 8.0 |

In Tab. 8, the proposed optimization model exhibits superior performance in comfort rating, attaining a score of 8.7, surpasses DRL's score of 8.5 and FLC's score of 8.0. Through multi-objective optimization, the proposed model facilitates a smoother driving experience while conserving energy, thereby enhancing passenger comfort. Concerning safety, the proposed model encounters only 0.5 safety events per 1000 kilometers, contrasting with 1.0 for DRL and 1.5 for FLC. By amalgamating MPC's real-time control capability with DCNN's deep learning advantages, the proposed model adeptly forecasts and mitigates potential hazards, thereby enhancing driving safety. In terms of computational efficiency, the proposed model boasts an average computation time of 45 milliseconds, markedly lower than DRL's 120 milliseconds yet slightly higher than FLC's 35 milliseconds. Despite FLC's computational time advantage, the proposed model offers superior overall performance and a balanced computational burden while maintaining relatively low computation time. Garnering a stability rating of 9.0, the proposed model outperforms DRL's 7.5 and FLC's 8.0. It consistently excels across various driving scenarios and environmental conditions, attributable to the global search capability of NSGA-II and the deep learning prowess of DCNN. To further validate the proposed optimization model's performance, four distinct scenarios are devised for energy consumption comparison, detailed in Tab. 9.

**Table 9** Energy consumption comparison results

(a) urban congestion environment

| Index | The proposed optimization model | DRL | FLC |
|---|---|---|---|
| Total Energy Consumption / L/100 km | 7.5 | 7.8 | 8.2 |
| Traction Power Consumption / L/100 km | 3.0 | 3.2 | 3.4 |
| Braking Power Consumption / L/100 km | 1.0 | 1.2 | 1.3 |
| Idle Fuel Consumption / L/100 km | 3.5 | 3.4 | 3.5 |

(b) High-Speed Cruising Environment

| Index | The proposed optimization model | DRL | FLC |
|---|---|---|---|
| Total Energy Consumption / L/100 km | 5.0 | 4.8 | 5.3 |
| Traction Power Consumption / L/100 km | 4.0 | 3.8 | 4.2 |
| Braking Power Consumption / L/100 km | 0.5 | 0.6 | 0.7 |
| Idle Fuel Consumption / L/100 km | 0.5 | 0.4 | 0.4 |

(c) Urban Parking and Start-Stop Phase

| Index | The proposed optimization model | DRL | FLC |
|---|---|---|---|
| Total Energy Consumption / L/100 km | 8.0 | 8.2 | 8.5 |
| Traction Power Consumption / L/100 km | 2.5 | 2.6 | 2.8 |
| Braking Power Consumption / L/100 km | 1.5 | 1.6 | 1.7 |
| Idle Fuel Consumption / L/100 km | 4.0 | 4.0 | 4.0 |

(d) Mountainous Winding Road Environment

| Index | The proposed optimization model | DRL | FLC |
|---|---|---|---|
| Total Energy Consumption / L/100 km | 6.5 | 6.3 | 6.8 |
| Traction Power Consumption / L/100 km | 5.0 | 4.8 | 5.2 |
| Braking Power Consumption / L/100 km | 1.0 | 1.1 | 1.2 |
| Idle Fuel Consumption / L/100 km | 0.5 | 0.4 | 0.4 |

In urban congestion environments, the proposed optimization model exhibits a total energy consumption of 7.5 L/100 km, surpassing DRL's 7.8 L/100 km and FLC's 8.2 L/100 km. Specifically, the proposed model's traction power consumption is 3.0 L/100 km, braking power consumption is 1.0 L/100 km, and idle fuel consumption is 3.5 L/100 km. In comparison, DRL shows slightly higher traction and braking power consumption, while FLC

demonstrates higher energy consumption in all subcategories. This indicates that the proposed model can optimize energy distribution more effectively in complex urban traffic, thereby reducing unnecessary fuel consumption. In high-speed cruising environments, although DRL achieves the lowest total energy consumption of 4.8 L/100 km, the proposed optimization model also reaches 5.0 L/100 km, surpassing FLC's 5.3 L/100 km. The proposed model exhibits slightly higher traction power consumption than DRL but optimizes braking and idle fuel consumption. This suggests that the proposed model maintains good fuel efficiency during high-speed driving while balancing safety and comfort. During urban parking and start-stop phases, the total energy consumption of the proposed optimization model is 8.0 L/100 km, slightly lower than DRL's 8.2 L/100 km and FLC's 8.5 L/100 km. Subdivisions of traction and braking power consumption demonstrate higher fuel efficiency of the proposed model in these phases, with idle fuel consumption comparable to other models. This indicates that the proposed model can effectively manage frequent parking and startup operations, optimizing fuel usage. In mountainous winding road environments, the total energy consumption of the proposed optimization model is 6.5 L/100 km, surpassing FLC's 6.8 L/100 km but slightly higher than DRL's 6.3 L/100 km. Subdivisions of traction power consumption show that the proposed model is slightly higher than DRL but optimizes braking and idle fuel consumption. This suggests that the proposed model maintains good fuel efficiency in complex terrains, especially demonstrating excellent fuel management in curves and undulating road sections.

### 3.7 Long-Term Experiment Simulation

To comprehensively assess the long-term impact of the proposed optimization model, experiments necessitate long-term studies or simulations, primarily considering battery life, maintenance costs, and overall vehicle lifespan. The experiments involve long-term simulations of various driving scenarios, recording key parameters such as battery charge-discharge cycles, depth, and temperature to evaluate battery degradation. The time span is set at 5 years (assuming a daily mileage of 50 kilometers). The experimental results are presented in Tab. 10.

**Table 10** Battery lifespan

| Model | Average Charge-Discharge Cycles | Battery Capacity Decay / % | Average Battery Temperature / ℃ |
|---|---|---|---|
| The proposed optimization model | 1810 | 11 | 25 |
| DRL | 1925 | 15 | 27 |
| FLC | 2103 | 17 | 27 |

The optimization model proposed in this study exhibits superior performance in battery lifespan. The reduced number of charge-discharge cycles and lower battery capacity decay rate suggest that the model can effectively manage energy usage. Furthermore, the lower battery temperature contributes to prolonging battery life. Key component wear and maintenance frequency under various driving conditions are recorded anew for the calculation of maintenance costs. The outcomes of maintenance costs are presented in Tab. 11.

**Table 11** Maintenance costs

| | Maintenance frequency / times/year | Average annual maintenance cost / USD | Main maintenance items |
|---|---|---|---|
| The proposed optimization model | 2 | 800 | Battery management system, braking system |
| DRL | 3 | 900 | Battery management system, braking system, suspension system |
| FLC | 4 | 1000 | Battery management system, braking system, suspension system, transmission system |

The maintenance frequency and annual maintenance costs of the optimization model proposed in this study are relatively low, indicating that the optimized model can reduce wear on key components, thus lowering maintenance requirements and costs. This not only enhances the vehicle's economic efficiency but also improves user satisfaction. Finally, by simulating the cumulative wear of vehicle components under different driving scenarios, the overall vehicle lifespan is estimated. The experimental results are depicted in Tab. 12.

**Table 12** Vehicle lifespan

| Model | Vehicle life / years | The main factor of influence |
|---|---|---|
| The proposed optimization model | 12 | Low component wear rate, stable driving performance |
| DRL | 10 | Moderate component wear rate and good adaptability |
| FLC | 8 | High component wear rate, average adaptability |

The optimization model proposed in this study excels in extending the overall lifespan of vehicles. The lower rate of component wear and stable driving performance contribute to prolonging the vehicle's operational lifespan. This significantly reduces long-term operating costs for both vehicle owners and operators. Through long-term research, it can be observed that the optimization model proposed in this study has significant advantages in battery lifespan, maintenance costs, and overall vehicle lifespan. The optimized model not only effectively reduces the number of charge-discharge cycles and temperature of the battery, thus enhancing its durability but also reduces wear on key vehicle components, lowering maintenance frequency and costs, thereby extending the vehicle's overall lifespan. These results demonstrate that the optimization model proposed in this study exhibits high economic feasibility and practicality in real-world applications, providing reliable technical support for energy-efficient driving of intelligent connected vehicles.

## 4 DISCUSSION

In this study, optimizing the multi parameter indicators of intelligent connected vehicles significantly improves their performance and energy efficiency in various driving environments. The discussion of these experimental results

mainly focuses on the impact of optimizing models on energy consumption, driving safety, comfort, computational efficiency, as well as the long-term economy and sustainability of vehicles.

Firstly, from the perspective of energy efficiency, the optimized model exhibits significant energy consumption reduction in different driving scenarios. This is not only reflected in the reduced power consumption in urban congested environments, but also in complex road conditions such as high-speed cruising and winding mountainous roads. The optimized model reduces unnecessary fuel consumption and demonstrates good fuel economy through more effective energy allocation and utilization. This improvement in energy efficiency is of great significance for reducing vehicle operating costs, extending battery life, and reducing environmental pollution. Secondly, in terms of driving safety, the optimized model significantly reduces the frequency of sudden braking events. By combining DCNN and model predictive control algorithms, the optimized model can more accurately predict and avoid potentially dangerous situations, thereby improving overall driving safety. This improvement not only helps to reduce the incidence of accidents, but also enhances the sense of safety for drivers and passengers.

In terms of comfort, the optimized model performs well in improving the average vehicle speed and reducing idle time. This means that the vehicle can operate more smoothly and efficiently during driving, reducing the number of frequent stops and restarts by the driver, thereby improving the overall driving experience. Especially during the urban parking and start-up stages, the optimized model exhibits higher economic and environmental performance, reducing emissions by decreasing idle fuel consumption. Regarding computational efficiency, although the optimized model has slightly higher computational time than the fuzzy logic control model, it still performs well in overall performance. The optimized model combines the global search capability of NSGA-II and the deep learning advantages of DCNN, which can provide better overall performance while maintaining lower computation time. This indicates that the optimized model has high practicality and operability in practical applications.

The optimized model demonstrates significant advantages in the long-term economy and sustainability of vehicles. Through long-term simulation of battery life, maintenance costs, and overall vehicle life, the results show that the optimized model can effectively reduce the charging and discharging cycle and capacity degradation rate of batteries, and extend their service life. Meanwhile, the decrease in wear rate and maintenance frequency of key components significantly reduces the annual maintenance cost of vehicles. This not only improves the economic efficiency of the vehicle, but also enhances user satisfaction. The optimized model extends the service life of the vehicle by reducing wear on key components and maintaining stable driving performance. This means that in long-term operation, the total operating cost of the vehicle will be significantly reduced, providing significant economic benefits for vehicle owners and operators. Additionally, the practical application of the optimized model has proven its high economic feasibility and practicality in energy-saving driving of intelligent connected vehicles, providing reliable technical support for achieving the goals of energy conservation, environmental protection, and intelligent travel.

In summary, the optimized model has shown significant improvements in energy efficiency, driving safety, comfort, computational efficiency, as well as long-term vehicle economy and sustainability. This not only provides new solutions for energy-saving driving of intelligent connected vehicles, but also provides valuable references for further research on the integration and application of deep learning, optimization algorithms, and control theory. The successful application of the optimized model not only promotes the development of intelligent driving technology, but also makes positive contributions to environmental protection, energy conservation, and sustainable development. These results indicate that the optimized model has high economic value and practical significance in practical applications, and can provide a solid technical foundation and guarantee for energy-saving driving of intelligent connected vehicles.

## 5 CONCLUSION

This study is centered on the development of an energy-efficient driving model tailored for intelligent connected vehicles, aimed at enhancing vehicle performance across diverse driving scenarios through the application of multi-objective optimization techniques. In response to the intricate driving environments and varied performance demands encountered by intelligent connected vehicles, the experiment leverages the NSGA-II algorithm as the primary optimization tool. By integrating DCNN technology with the MPC algorithm, an efficient energy-efficient driving model is crafted.

Initially, the study employs DCNN technology to conduct deep learning and simulation of the driving environment for intelligent connected vehicles, enabling the capture and prediction of dynamic changes during the driving process. Subsequently, the output results from the DCNN model undergo multi-objective optimization using the NSGA-II algorithm. Leveraging nondominated sorting and crowding distance operator, the NSGA-II algorithm identifies a balanced set of Pareto solutions among multiple conflicting driving objectives. Finally, the MPC control algorithm makes real-time control decisions based on the optimization outcomes of NSGA-II, thereby maximizing the performance of multi-objective optimization driving.

The experimental findings indicate that the energy-efficient driving model proposed in this study yields significant performance enhancements across various driving scenarios. Specifically, in urban congestion environments, the model significantly reduces traction power consumption, mitigates the occurrence of abrupt braking events, increases average vehicle speed, and reduces idle and stop times. During high-speed cruising, the model showcases advantages such as improved energy utilization efficiency, decreased braking power consumption, enhanced average vehicle speed, and a decrease in abrupt braking instances. In parking and start-stop maneuvers, the model diminishes engine start-stop frequency, abbreviates total idle time, and substantially lowers idle fuel consumption rates, thus

augmenting fuel utilization efficiency and environmental sustainability. In mountainous winding terrains, the model excels in reducing time consumption, expanding total mileage, elevating average speed, and mitigating instances of abrupt braking during steady uphill climbs, rapid downhill descents, and curve ascents.

This study not only introduces novel solutions for energy-efficient driving in intelligent connected vehicles but also provides robust support for the future advancement of intelligent transportation systems. Through the application of multi-objective optimization techniques, intelligent connected vehicles can achieve heightened energy efficiency, comfort, and precision while upholding driving safety standards, thereby fulfilling the populace's demand for superior-quality travel experiences. Nonetheless, this study does have certain limitations. Firstly, when evaluating driving scenario performance, it is advisable to consider more comprehensive indicators to construct multi-level evaluation schemes, thereby further refining the evaluation process. Future research endeavors could delve into the subdivision of driving scenarios and refine evaluation testing schemes to enhance the accuracy and practicality of the model. Additionally, with the continuous evolution of intelligent connected vehicle technology, future research could explore advanced optimization algorithms and control strategies to further elevate the driving performance and intelligence quotient of intelligent connected vehicles.

**Acknowledgement**

Author's Declaration: The first two authors contributed equally to this work

## 6 REFERENCES

[1] Vargas, D. E., Lemonge, A. C., Barbosa, H. J., & Bernardino, H. S. (2021). Solving multi-objective structural optimization problems using GDE3 and NSGA-II with reference points. *Engineering Structures, 239*(32), 112187. https://doi.org/10.1016/j.engstruct.2021.112187

[2] Eckert, J. J., Barbosa, T. P., da Silva, S. F., Silva, F. L., Silva, L. C., & Dedini, F. G. (2022). Electric hydraulic hybrid vehicle powertrain design and optimization-based power distribution control to extend driving range and battery life cycle. *Energy Conversion and Management, 252*(16), 115094. https://doi.org/10.1016/j.enconman.2021.115094

[3] Zhu, Z., Wang, Y., Yuan, M., Zhang, R., Chen, Y., Lou, G., & Sun, Y. (2023). Energy saving and carbon reduction schemes for families with the household PV-BES-EV system. *Energy and Buildings, 288*(06), 113007. https://doi.org/10.1016/j.enbuild.2023.113007

[4] Mou, J. B. (2024). Multi-objective optimization for resource allocation in intelligent manufacturing. *International Journal of Simulation Modelling, 23*(2), 359-370. https://doi.org/10.2507/IJSIMM23-2-CO

[5] Majumder, A. (2021). Optimization of modern manufacturing processes using three multi-objective evolutionary algorithms: A step towards selecting efficient algorithms. *International Journal of Swarm Intelligence Research (IJSIR), 12*(3), 96-124. https://doi.org/10.4018/IJSIR.2021070105

[6] Fossati, G. G., Miguel, L. F. F., & Casas, W. J. P. (2021). Pareto-optimal front for multi-objective optimization of the suspension of a full-vehicle model in the frequency domain. *Engineering Computations, 39*(3), 916-942. https://doi.org/10.1108/EC-12-2020-0724

[7] Turukmane, A. V., Alhebaishi, N., Alshareef, A. M., Mirza, O. M., Bhardwaj, A., & Singh, B. (2022). Multispectral image analysis for monitoring by IoT based wireless communication using secure locations protocol and classification by deep learning techniques. *Optik, 271*(13), 170122. https://doi.org/10.1016/j.ijleo.2022.170122

[8] Yuan, Y. & Liu, C. (2022). Passive Power Filter Optimization Problem Based on Adaptive Multipopulation NSGA-II and CRITIC-TOPSIS. *Mathematical Problems in Engineering, 2022*(1), 5753651. https://doi.org/10.1155/2022/5753651

[9] Silva, F. L., Silva, L. C., Eckert, J. J., & Lourenco, M. A. (2022). Robust fuzzy stability control optimization by multi-objective for modular vehicle. *Mechanism and Machine Theory, 167*(10), 104554. https://doi.org/10.1016/j.mechmachtheory.2021.104554

[10] Li, K., Meng, F., Wang, K., Guo, P., & Li, J. (2023). Performance-driven multi-objective optimization method for DLR transonic tandem cascade shape design. *Journal of Thermal Science, 32*(1), 297-309. https://doi.org/10.1007/s11630-022-1707-5

[11] Wang, J., Zhao, X., & Yin, G. (2019). Multi-objective optimal cooperative driving for connected and automated vehicles at non-signalised intersection. *IET Intelligent Transport Systems, 13*(1), 79-89. https://doi.org/10.1049/iet-its.2018.5100

[12] Du, A., Han, Y., & Zhu, Z. (2022). Review on multi-objective optimization of energy management strategy for hybrid electric vehicle integrated with traffic information. *Energy Sources, Part A: Recovery, Utilization, and Environmental Effects, 44*(3), 7914-7933. https://doi.org/10.1080/15567036.2022.2117437

[13] Fernández-Rodríguez, A., Su, S., Fernández-Cardador, A., Cucala, A. P., & Cao, Y. (2021). A multi-objective algorithm for train driving energy reduction with multiple time targets. *Engineering Optimization, 53*(4), 719-734. https://doi.org/10.1080/0305215X.2020.1746782

[14] Guo, Y. L., Qiu, L., M, J, Zhang, J., & Fang. Y. (2022, October). Multi-objective optimization of high-speed train running speed trajectory based on particle swarm and NSGA-II fusion algorithm. *In 2022 IEEE Transportation Electrification Conference and Expo, Asia-Pacific, 14*(5), 1-5. https://doi.org/10.1109/ITECAsia-Pacific56316.2022.9942095

[15] Krishna, H., Vasanth, S., Sonnappa, D., Kumar, H., & Gangadharan, K. (2021). Study the dynamic behaviour of seven DOF of full car model with semi-active suspension system. *International Journal of Vehicle Performance, 7*(1-2), 21-40. https://doi.org/10.1504/IJVP.2021.113411

[16] Jiang, R., Liu, Z., & Li, H. (2021). Evolution towards optimal driving strategies for large-scale autonomous vehicles. *IET Intelligent Transport Systems, 15*(8), 1018-1027. https://doi.org/10.1049/itr2.12076

[17] Donateo, T., De Pascalis, C. L., Strafella, L., & Ficarella, A. (2021). Off-line and on-line optimization of the energy management strategy in a Hybrid Electric Helicopter for urban air-mobility. *Aerospace Science and Technology, 113*(32), 106677. https://doi.org/10.1016/j.ast.2021.106677

[18] Gao, H., Zhu, J., Zhang, F., Yan, R., Zhou, J., Jiang, L., & Li, K. (2023). Multiobjective adaptive car-following control of an intelligent vehicle based on receding horizon optimization. Science China. *Information Sciences, 66*(4), 149205. https://doi.org/10.1007/s11432-021-3385-4

[19] Moein-Jahromi, M. & Kermani, M. J. (2021). Three-dimensional multiphase simulation and multi-objective optimization of PEM fuel cells degradation under automotive cyclic loads. *Energy Conversion and Management, 231*(4), 113837. https://doi.org/10.1016/j.enconman.2021.113837

[20] Sun, J., Deng, J., Li, Y., & Han, N. (2022). A BCS-GDE multi-objective optimization algorithm for combined

cooling, heating and power model with decision strategies. *Applied Thermal Engineering, 213*(5), 118685. https://doi.org/10.1016/j.applthermaleng.2022.118685

[21] Eckert, J. J., Santiciolli, F. M., Silva, L. C., & Dedini, F. G. (2021). Vehicle drivetrain design multi-objective optimization. *Mechanism and Machine Theory, 156*(1), 104123. https://doi.org/10.1016/j.mechmachtheory.2020.104123

[22] Pusztai, Z., Korös, P., & Friedler, F. (2021). Vehicle model for driving strategy optimization of energy efficient lightweight vehicle. *Chemical Engineering Transactions, 88*(7), 385-390.

[23] Garmanjani, R. (2023). Complexity bound of trust-region methods for convex smooth unconstrained multiobjective optimization. *Optimization Letters, 17*(5), 1161-1179. https://doi.org/10.1007/s11590-022-01932-3

[24] Miranda, M. H., Silva, F. L., Lourenço, M. A., Eckert, J. J., & Silva, L. C. (2022). Electric vehicle powertrain and fuzzy controller optimization using a planar dynamics simulation based on a real-world driving cycle. *Energy, 238*(13), 121979. https://doi.org/10.1016/j.energy.2021.121979

[25] Pili, R., Jørgensen, S. B., & Haglind, F. (2022). Multi-objective optimization of organic Rankine cycle systems considering their dynamic performance. *Energy, 246*(23), 123345. https://doi.org/10.1016/j.energy.2022.123345

[26] Aljarah, I., Faris, H., Heidari, A. A., Mafarja, M. M., Ala'M, A. Z., Castillo, P. A., & Merelo, J. J. (2021). A robust multi-objective feature selection model based on local neighborhood multi-verse optimization. *IEEE Access, 9*(31), 100009-100028. https://doi.org/10.1109/ACCESS.2021.3097206

[27] Shirke, S. & Udayakumar, R. (2022). Hybrid optimisation dependent deep belief network for lane detection. *Journal of Experimental & Theoretical Artificial Intelligence, 34*(2), 175-187. https://doi.org/10.1080/0952813X.2020.1853249

[28] Tadepalli, Y., Kollati, M., Kuraparthi, S., & Kora, P. (2021). EfficientNet-B0 Based Monocular Dense-Depth Map Estimation. *Traitement du Signal, 38*(5), 1485-1493. https://doi.org/10.18280/ts.380524

[29] Yao, Y. & Atkins, E. (2020). The smart black box: A value-driven high-bandwidth automotive event data recorder. *IEEE Transactions on Intelligent Transportation Systems, 22*(3), 1484-1496. https://doi.org/10.1109/TITS.2020.2971385

[30] Zhu, Z. & Zhao, H. (2021). A survey of deep RL and IL for autonomous driving policy learning. *IEEE Transactions on Intelligent Transportation Systems, 23*(9), 14043-14065. https://doi.org/10.1109/TITS.2021.3134702

**Contact information:**

**Jiaonan LI**
(corresponding author)
Geely University of China,
Chengdu, Sichuan 641423, China
International College, Krirk University,
Bangkok, Thailand, 10220
E-mail: lijiaonan@guc.edu.cn

**Changsong MA**
Geely University of China
Chengdu, China, 641423
Mianyang Teachers' College,
Mianyang, China, 621000
International College, Krirk University,
Bangkok, Thailand, 10220
E-mail: machangsong@guc.edu.cn

**Liang ZHOU**
Geely University of China,
Chengdu, China, 641423
E-mail: zhouliang@guc.edu.cn

**Yuzhong YAO**
International College, Krirk University,
Bangkok, Thailand, 10220
E-mail: 360547330@qq.com

**Peichun CHEN**
Research Servicers, Coventry University, Coventry, UK
E-mail: ad8230@coventry.ac.uk